Adaptive optics scanning laser ophthalmoscopy for *in vivo* imaging of lamina cribrosa

**Abhiram S. Vilupuru,* Nalini V. Rangaswamy, Laura J. Frishman, Earl L. Smith III,
Ronald S. Harwerth, and Austin Roorda†**

505 J. Davis Armistead Building, College of Optometry, University of Houston, Houston, Texas 77204-2020, USA

The lamina cribrosa has been postulated from *in vitro* studies as an early site of damage in glaucoma. Prior *in vivo* measures of laminar morphology have been confounded by ocular aberrations. In this study the lamina cribrosa was imaged after correcting for ocular aberrations using the adaptive optics scanning laser ophthalmoscope (AOSLO) in normal and glaucomatous eyes of rhesus monkeys. All measured laminar morphological parameters showed increased magnitudes in glaucomatous eyes relative to fellow control eyes, indicating altered structure. The AOSLO provides high-quality images of the lamina cribrosa and may have potential as a tool for early identification of glaucoma. © 2007 Optical Society of America

OCIS codes: 010.1080, 170.5810, 170.4470, 170.4730, 170.4580.

1. INTRODUCTION

Glaucoma is described clinically as a multifactorial disease that ultimately leads to the death of retinal ganglion cells (RGCs). RGC axons pass through a sieve-like structure, the lamina cribrosa, in the optic nerve head, forming the optic nerve that conveys visual information to the brain. RGC axonal health is intimately dependent on the normal structure and function of the lamina cribrosa.[1–3] Previous *in vitro* and postmortem histological studies on human and monkey glaucomatous eyes have shown early pathological alterations in the lamina cribrosa morphology, connective tissue support structure, and cellular architecture.[1,4–17] Changes in the lamina cribrosa morphology have been shown to disrupt ganglion cell axons traversing the structure, causing blockage of axoplasmic flow or even mechanical nipping of the axons.[1,2,5,18–25] These prior studies of laminar morphology in glaucomatous eyes of humans and macaques with experimental glaucoma have provided important information about the pathophysiology of glaucoma. However, studying laminar morphology *in vivo* would have an additional benefit of tracking changes over time. Prior *in vivo* studies of lamina cribrosa in normal and glaucomatous eyes have been conducted using optic disc photography[26] and confocal scanning laser ophthalmoscopy.[27–32] Bhandari *et al.*[31] and Fontana *et al.*,[32] in particular, modified the confocal SLO in an effort to better visualize laminar pores.[29–32] For these studies, they selected subjects whose lamina was visible with biomicroscopy to facilitate imaging, possibly because the presence of ocular aberrations[33] limited the confocality of their SLO. To study the benefits of increased image quality the main aim of our study was to image the lamina cribrosa after correcting ocular aberrations using an adaptive optics confocal scanning laser ophthalmoscope (AOSLO).

In the AOSLO, ocular aberrations[33] are corrected online during retinal imaging by a deformable mirror, thereby improving image quality. The specific instrument has been described in detail elsewhere.[34] The use of adaptive optics to correct ocular aberrations greatly improves resolution, increases throughput or amount of light reaching the detector, and increases contrast by limiting the light in the image to that which comes from the plane of focus. The AOSLO has been used previously for imaging photoreceptors, retinal vasculature, and blood flow velocity in foveal capillaries.[35–38] Adaptive optics also improves confocal optical sectioning ability by focusing the light from the surface of interest to a smaller spot. The confocal aperture can therefore be smaller in an AOSLO than in a regular confocal SLO, thereby improving optical sectioning. Improved optical sectioning is important in imaging of the lamina cribrosa because the optic nerve head is a complex structure that contains connective tissue, astrocytes, and incoming axons overlying lamina cribrosa.

Rhesus monkeys with experimental glaucoma induced in one eye, leaving the fellow eye as a control, were used as subjects in our study. The monkey model of experimental glaucoma has been used extensively, and previous studies have clearly established its validity and advantages.[5,8,9,16–21,24,39–41] To our knowledge, this is the first study of high-resolution imaging of the primate optic nerve head using the AOSLO; our aim was to visualize and quantify laminar morphological changes associated with glaucoma.

2. METHODS

Four adult rhesus monkeys (*Macaca mulatta*), aged between 5 and 7 years were subjects in this study. All of the experimental and animal care procedures were reviewed and approved by the Institutional Animal Care and Use Committee (IACUC) of the University of Houston, and they adhered to the ARVO statement for Use of Animals in Ophthalmic and Vision Research. Unilateral laser-induced ocular hypertension was the experimental model of glaucoma.[39–42] The treatment procedures for induction

of ocular hypertension have been described in detail elsewhere[42] and will not be presented here. Ocular hypertension was induced in the right eyes of three of the four rhesus monkeys, while both eyes of one monkey remained untreated as a bilateral control for AOSLO imaging. All of these animals were subjects in other studies as well.

All imaging sessions were conducted after anesthetizing the monkey with ketamine $(20-25 \, \text{mg} \, \text{kg}^{-1}, \text{IM})$, xylazine $(0.8-0.9 \, \text{mg} \, \text{kg}^{-1}, \text{IM})$ and atropine sulfate $(0.04 \, \text{mg/kg}, \text{SC})$.[43] The anesthetic mixture is effective in minimizing eye movements.[43] The pupils were dilated with 2.5% phenylephrine, 1% tropicamide, and imaging was conducted after maximum dilation was achieved. The monkey was placed in a head holder that was attached to a 5-degree-of-motion (*X-Y-Z* tip tilt) goniometer stage that allowed for translation of the pupil as well as tip and tilt of the monkey's eye about the pupil center. This allowed us to align the head in order to center and visualize the optic nerve head since eye movements were arrested by anesthesia.[43] The eye to be imaged was held open using a lid speculum; a contact lens, with 1% methyl cellulose in its sag, was placed on the cornea to prevent loss of optical clarity due to corneal dehydration. The wavelength of the scanning laser was 660 nm, and the field of view of the instrument was 2.5 deg $(512 \times 480 \text{ pixels})$ for all the imaging sessions. The laser power at the eye was of the order of $20 \, \mu\text{W}$, and the beam diameter was 5.9 mm. The subjects' refractive errors were corrected to the nearest 0.25 diopter (dB) with spherical and cylindrical trial lenses placed at the spectacle plane. Ocular aberrations were measured at the retinal eccentricity of the optic nerve head using the Shack–Hartmann wavefront sensor[33] in the AOSLO. If the optic nerve head had, for example, a large cupping causing weak backscattering of light from the lamina cribrosa, aberrations were measured at a retinal location beside the optic nerve head. Aberrations were corrected using a 37-channel deformable mirror (Xinetics, Inc., Devens, Massachusetts). Correction of the aberrations (adaptive optics compensation) was achieved at a frequency of 5 Hz so that compensation occurred well within 1 s. The same light (660 nm) was used for both measurement of aberrations and imaging the lamina cribrosa. The adaptive optics compensation provided $\sim 2 \, \mu\text{m}$ lateral resolution and the ability to locate planes in the retina to better than $10 \, \mu\text{m}$ accuracy ($\sim 1/10$ of the axial resolution[36]), but each optical section included $100 \, \mu\text{m}$ of tissue. Confocal optics in the AOSLO were used to generate en-face axial sections of the optic nerve head from the surface of the optic nerve head to the lamina cribrosa. In this way the best plane to image the lamina cribrosa was identified, and video sequences of the lamina cribrosa were acquired at that plane and stored to a computer disk at a rate of 30 fps to be analyzed off line. Superior, central, and inferior laminar pores were imaged by appropriate alignment of the animal's head. After imaging of the lamina cribrosa of the first eye was completed, the second eye was prepared for imaging in the same fashion. Each imaging session lasted about 3 h for both eyes. The right eye of the monkey in which both eyes were normal was imaged on two different occasions to assess variability in our measurement or analysis. Both eyes of the other three monkeys were imaged once.
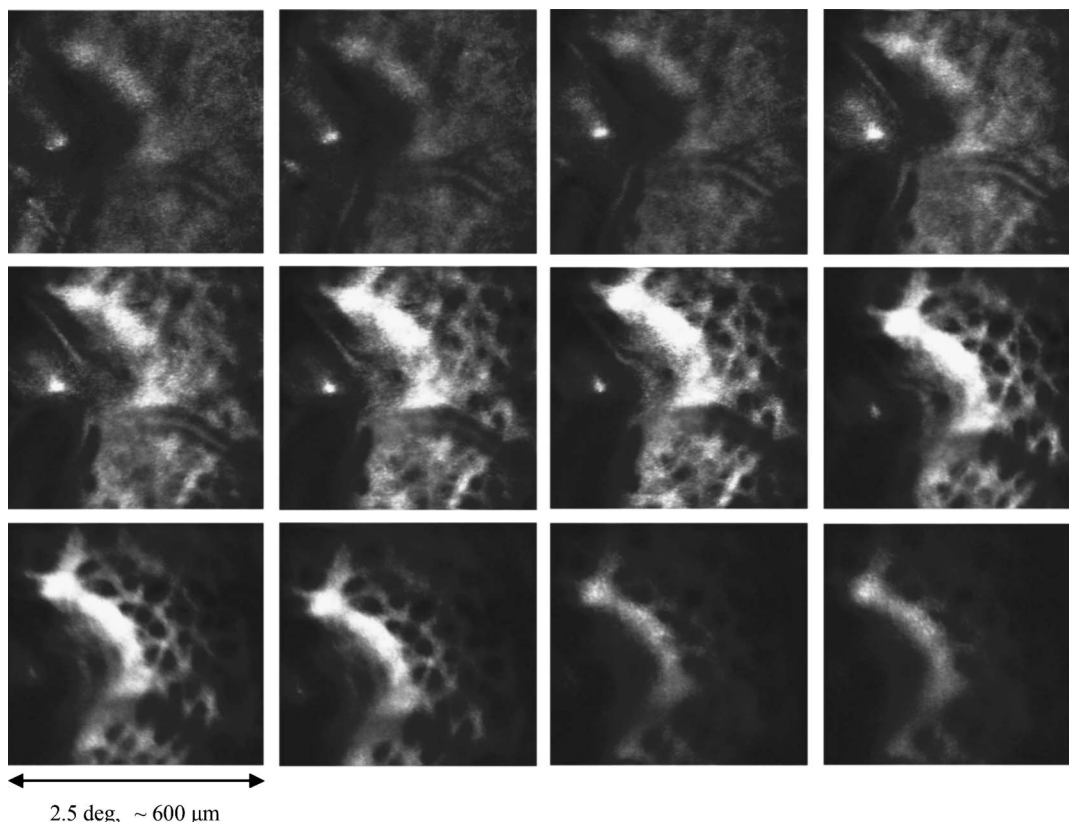

2.5 deg, ~ 600 μm

Fig. 1. Axial sections at the optic nerve head traveling in the anterior-to-posterior direction from the top left to bottom right frame. The focal plane for laminar analysis was identified by locating the plane at which the lamina was in best focus.
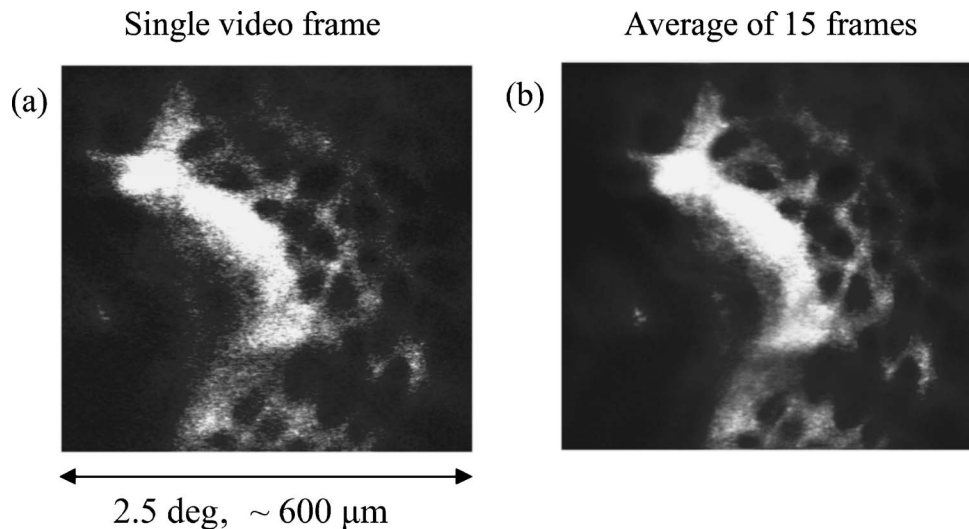
Fig. 2. (a) Single video frame showing the lamina cribrosa of the right eye of a monkey. This image illustrates the noise inherent in the single video image. Fifteen such frames were averaged to obtain better images [example shown in (b)], where signal to noise ratio was clearly improved by averaging. All subsequent figures in this paper subtend the same visual angle and represent the same physical distance on the retina.
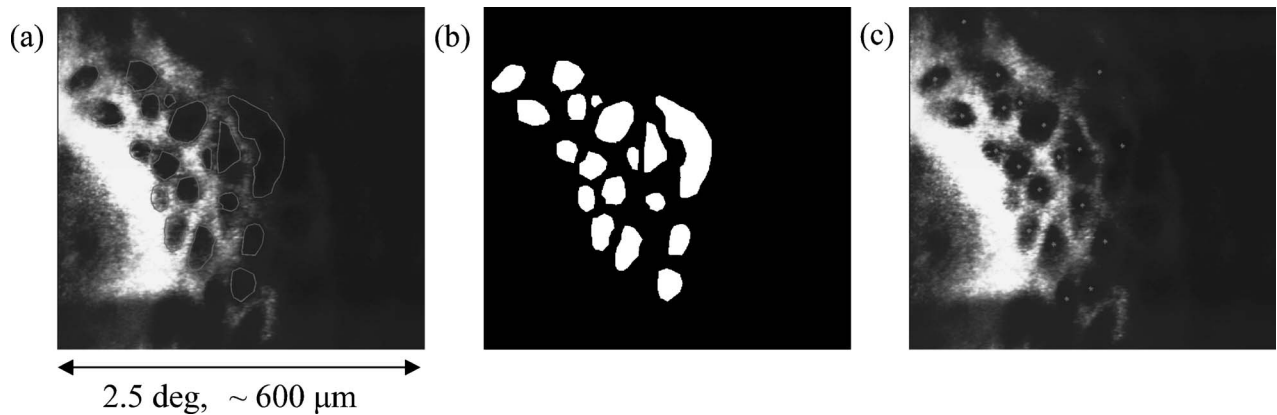

Fig. 3. (a) Polygons were drawn interactively around clearly demarcated and visible laminar pores in the averaged images. (b) The image was then binarized such that areas within the polygons were white while other areas were black. The binarization allows ImageTool image analysis software to automatically detect and measure areas and elongation of each laminar pore. (c) Nearest-neighbor distance was calculated by interactively identifying centers of each clearly demarcated laminar pore.

Figure 1 demonstrates the confocal ability of the AOSLO to produce axial sections of the optic nerve head. The images are averaged frames at each axial location, and axial sectioning was performed in an anterior–posterior direction from top left to bottom right frame. In off-line analysis, using a custom-written MATLAB program, first a reference frame was selected from each segment of video. The reference frame was automatically selected as the one with highest average intensity, since relative intensity has been shown to be correlated with image quality.[35] All frames in the sequence were then shifted to find the best cross correlation with the reference. The 15 best-correlated frames (highest correlation coefficient) in the video sequence of the lamina cribrosa were selected, automatically shifted, and averaged to reduce noise in the image.[35] Figure 2 illustrates the benefit of averaging video frames to reduce noise in the image. All further laminar pore analysis was conducted on averaged images. Area and elongation (major axis length/minor axis length) of each pore were measured using a custom written MATLAB software. These two parameters have been used in

previous studies of the lamina cribrosa to quantify differences between normal and glaucomatous eyes.[32] We also measured nearest-neighbor distance as the distance of the nearest pore from each pore.[44] This parameter would indicate change in the lamina during experimental glaucoma even if pore size or elongation did not change.

Each clearly visible laminar pore was identified, and a polygon was drawn interactively around its edges by an observer [Fig. 3(a)]. When all the laminar pores were identified, the resulting image with polygons overlying the pores was binarized so that laminar pores would be white and all other areas of the image would be black [Fig. 3(b)]. This image was exported to ImageTool (UTH-SCSA, ver. 3) image analysis software, which measured area and elongation of each pore in the image. Nearest-neighbor distance was measured using a custom-written MATLAB program by interactively marking centers of visible laminar pores and calculating the nearest pore to each of the laminar pores [Fig. 3(c)]. All clearly demarcated and visible laminar pores were measured in each eye of the four monkeys. Although some pores would be
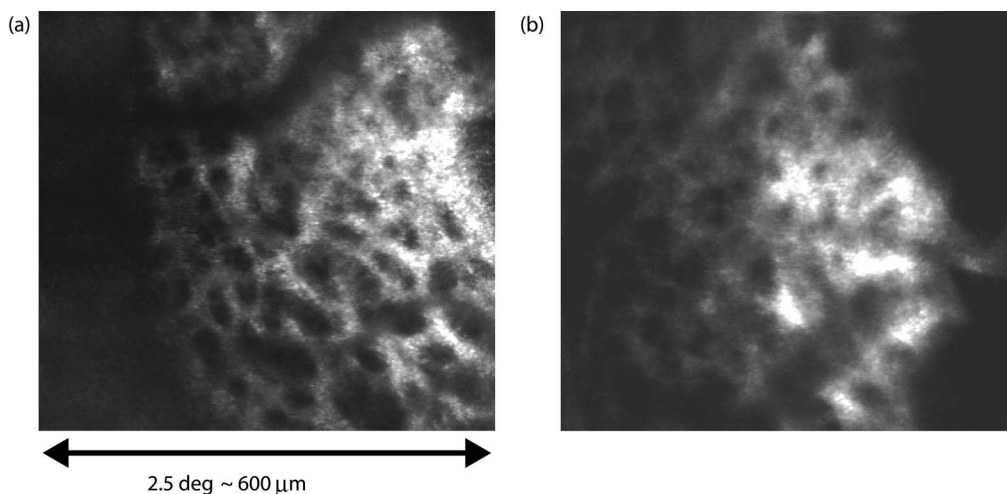
Fig. 4.   Lamina cribrosa images from two normal (left) eyes of two monkeys. Laminar pores are clearly visible in both cases.
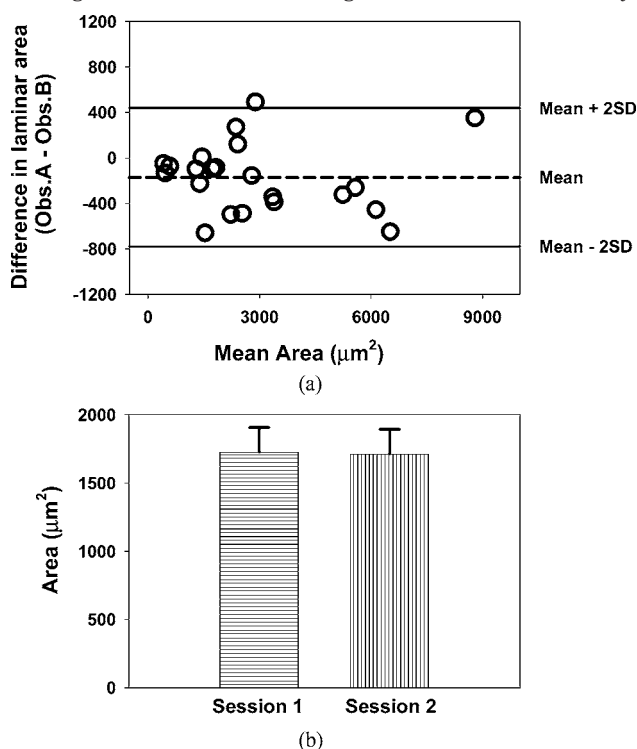

Fig. 5.   (a) Altman–Bland analysis of inter-observer variability in the measurement of laminar pore area for the same image. Difference between observers is plotted against mean of measurements. The solid line is mean of differences; dashed lines represent two standard deviations above and below the mean. (b) Plot of inter-session reproducibility of laminar area measurements. The vertical bars represent average laminar pore area; error bars show the standard error of the mean.

imaged in two different videos during any given imaging session, care was taken not to reanalyze the same pore. Average and standard errors of the mean were calculated for the three measured morphological parameters. Each glaucomatous right and normal left eye was imaged once; averages and standard errors of mean represent data from one imaging session.

A-scan ultrasonography was performed in all eyes of all monkeys to measure axial length. Morphological parameters obtained in measures of visual field angle were con-
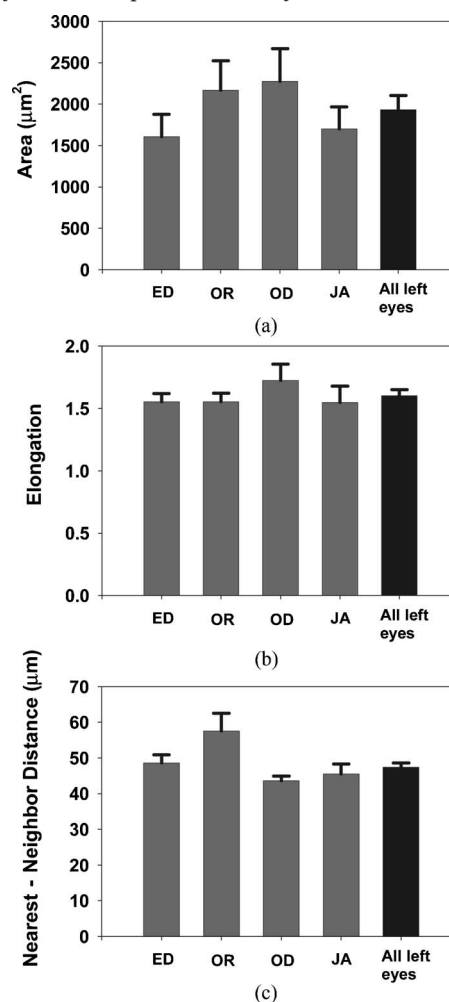

Fig. 6.   The three morphological parameters (area, elongation; and nearest-neighbor distance) measured in all control eyes of the four monkeys ED, OR, OD, and JA. In each graph the gray bars represent individual eyes and the black bar is the group average of all control eyes. The bars are means and the error bars show the standard error of the mean.

verted to true retinal size using the method described by Bennett *et al.*[45] using the measured axial lengths. Standard automated perimetry (SAP) was performed behav-

iorally on both eyes of each of the monkeys as part of other experiments conducted on these subjects. A Goldmann size III target was used with white-on-white contrast to estimate the mean deviation or average sensitivity difference from normal across the visual field. Mean deviation was used as a descriptor of the stage of experimental glaucoma in each of the eyes. The procedure has been described in detail elsewhere.[39–41]

3. RESULTS

Figure 4 shows the lamina cribrosa images of two normal eyes. The laminar pores are clearly visible and in focus at this axial location. These images have been averaged to reduce noise as described above (see Fig. 2). Before the results are reported for glaucomatous eyes, data will be presented on inter-observer variability and inter-session repeatability to validate the image analysis approach taken in this study.

Figure 5(a) presents an Altman–Bland plot for laminar pore area to assess degree of agreement between two observers. The figure shows difference in area between two observers versus mean of the two measurements from the two observers. The dashed line represents the mean of the differences, and the solid lines are two standard deviations from the mean. The finding that the mean difference was less than zero indicates that observer B, on average, measured larger areas than observer A. However, the difference was not significant compared with the magnitude of laminar pore areas ($p > 0.05$). In addition, there is no apparent trend in the differences between the two observers when greater magnitude of pores was measured. Figure 5(b) plots average laminar pore area for one normal eye measured at two different times separated by 60 days.

The error bars represent standard errors of mean. There was no statistically significant difference between the two measurements (t-test; $p = 0.95$), indicating good repeatability in both image acquisition and the analysis. Figure 6 presents data for average area, elongation, and nearest-neighbor distance for all four normal left eyes in four monkeys. In each plot, gray bars show the average for the normal left eye of each monkey and black bars show the average of all normal eyes. Although there was variability among the four left eyes, the difference was not statistically significant (ANOVA, $p = 0.3$).

Figure 7 shows examples of the lamina cribrosa of (a) an eye (right) with experimental glaucoma and (b) its fellow control (left). The eye with experimental glaucoma has, on average, larger and more elongated holes, signifying altered laminar morphology. The difference in mean deviation between the two eyes of this monkey according to behavioral SAP was 6.5 dB, which represents a moderate loss of sensitivity across the visual field. Differences in laminar morphology between the two eyes of all four monkeys are plotted in Fig. 8 for (a) average area, (b) elongation, and (c) nearest-neighbor distance. To reiterate, both eyes of monkey ED are normal, the difference in mean deviation between the two eyes of monkey OR is 6.88 dB, of monkey OD is 6.5 dB, and of monkey JA is 27.5 dB. The area of the laminar pores was significantly greater in the three experimental glaucoma eyes than in their respective normal fellow eyes (t-test; $p < 0.05$). Elongation was also systematically greater in experimental glaucoma eyes than in their counterparts, but statistical significance was reached only for monkey JA, which had end-stage experimental glaucoma. Similarly, nearest-neighbor distance was significantly greater for monkeys OD and JA but not for monkey OR. Elongation and
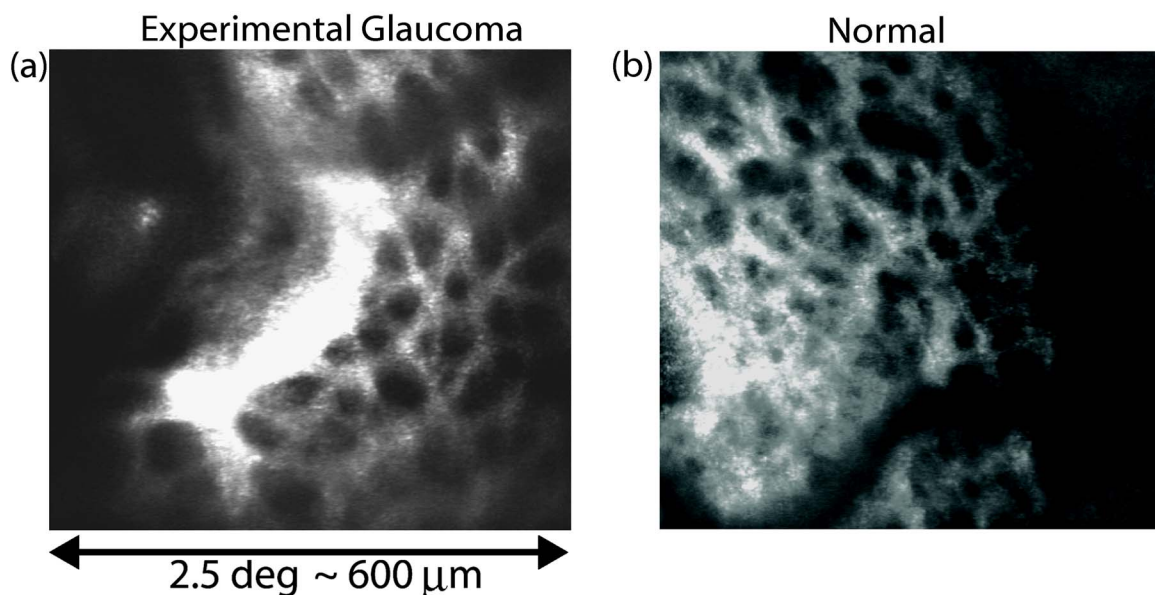

Fig. 7. (Color online) (a) Experimental glaucoma and (b) normal eyes of the same monkey (OD). In the two panels the central optic nerve head is imaged in the two eyes to compare the lamina cribrosa. The images illustrate that, on average, pores in the eye with experimental glaucoma have greater area and elongation than its normal fellow eye, indicating altered morphology in the glaucomatous eye.
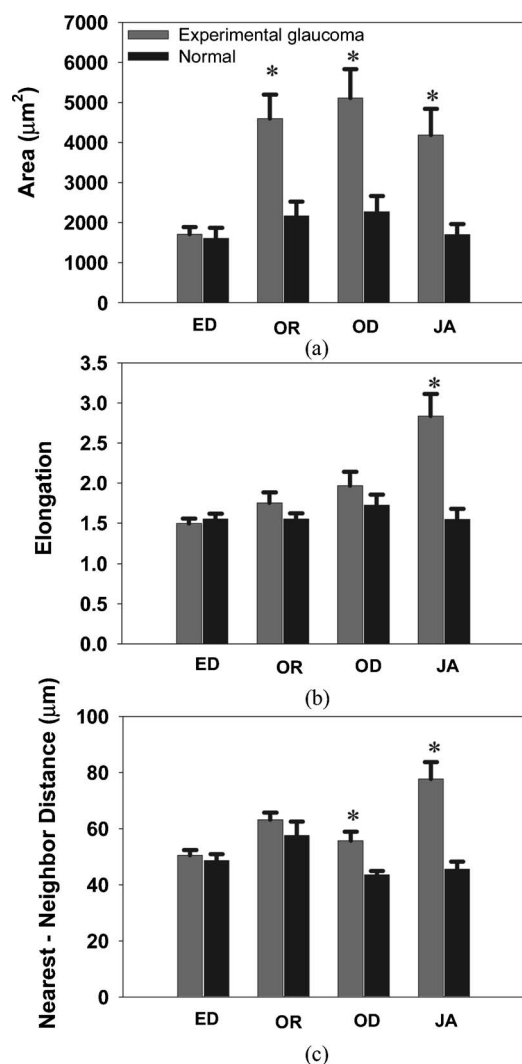
Fig. 8. (a) Average area, (b) elongation, and (c) nearest-neighbor distance comparisons between experimental glaucoma eyes (gray bars) and their contralateral (black bars) in all four monkeys. Bars plot average laminar morphology, error bars represent the standard error of the mean. Asterisks indicate that the difference is statistically significant.

nearest-neighbor distance were greater in the severely glaucomatous eye of monkey JA than in monkeys OR and OD with only moderate damage.

4. DISCUSSION

The AOSLO, a recently proposed imaging technology,[34] provided high-resolution, high-contrast, magnified images of lamina cribrosa in both normal and experimentally induced glaucomatous eyes. Prior *in vivo* studies of laminar morphological changes had measured differences between glaucomatous stages.[31,32]. However, the prior studies used a 20 deg field of view and were limited in obtaining higher-magnification and higher-resolution images because of ocular aberrations. In our study, laminar pores were imaged using a 2.5 deg window at a higher magnification, which provided details of the anterior laminar surface. In most eyes, ocular aberrations were corrected without much difficulty at the level of the optic

nerve head, but in some cases appropriate correction could not be achieved when the field of view used encompassed different depth planes. In such eyes, aberrations were measured at a retinal location adjacent to the optic nerve head and the same correction was applied to image the lamina cribrosa. AOSLO imaging of the lamina cribrosa developed in this study provides interesting preliminary data and justification for such studies of early structural changes in glaucoma in the future.

Imaging the lamina cribrosa may have important application in glaucoma, as it has been postulated to be the primary site of injury to ganglion cell axons, ultimately leading to death of ganglion cells and blindness.[1–24]Serial sectioning of the lamina cribrosa is illustrated in Fig. 1, demonstrating the ability of the AOSLO to optically section from the surface of the optic nerve head down to the lamina cribrosa. Confocal optical sectioning identified for further analysis the focal plane where the lamina cribrosa was at best focus. We presume that at this focal plane we are imaging the anterior laminar surface, because attempts to focus posterior to this surface reveal no new structure. Using the current technology we are unable to section the lamina cribrosa itself to measure pores at different depths.

The 2.5 deg window employed encompassed most of the visible laminar pores at the center of the disc. In addition, we moved the eye to image laminar pores at extreme superior and inferior aspects of the disc to capture all of the visible laminar surface. The averaged images were postprocessed to quantify laminar pores, ensuring that none of the pores was included more than once in the final analysis. Area and elongation of laminar pores were described in a previous study as differentiating between mild and severe glaucomatous stages.[32] In addition, we chose to measure nearest-neighbor distance, which has been used previously as a measure of randomness in a measurement sample.[44] Nearest-neighbor distance may be an effective identifier of change in laminar morphology when lamina cribrosa is affected, for example, by shear stress causing distortion of laminar surface.[4–7,14–17] In effect, we sought to provide analysis parameters that would detect the earliest alterations in laminar morphology.

Automated image analysis methodology was attempted as suggested in prior studies[31] to quantify the laminar morphology. However, applying similar analyses to our images failed to capture the details of the lamina visible to the observer because of the intensity variability within each image and between images. During each imaging session our aim was to obtain the best possible images of the lamina notwithstanding standardization of input luminance levels. Hence, even within the same eyes imaged on different dates, average intensity levels varied, and therefore interactive identification of laminar pores was always more reliable than automatic computerized image analysis to identify and measure area, elongation, and nearest-neighbor distance. This approach was validated by insignificant inter-observer variability and significant repeatability in laminar morphological measurements (Fig. 5).

Images of the lamina cribrosa in two normal eyes of two monkeys (Fig. 4) demonstrate inter-subject variability, which is reflected in the quantification in Fig. 6. The num-

ber of pores visible in the two normal eyes is different, and this may be because of differences in optic disc structure, since more pores are visible in larger optic discs than in smaller ones. High-magnification imaging using the AOSLO allows us to image a sufficient number of pores in any given optic disc hence obviating the need to select larger optic discs as was required for previous studies.[31,32] There was no statistical difference between any of the three measured parameters within the three normal eyes (Fig. 6). However, close inspection suggested subtle differences between aspects of laminar morphology quantified by them. For example subject OR has, on average, larger area and nearest-neighbor distance than subject ED, but elongation is similar between the two. Also, subject OD shows a slightly larger area and elongation than subject OR, but subject OR shows a greater nearest-neighbor distance than subject OD. Therefore the three parameters, although they describe morphology of the same structure, quantify different aspects of the laminar pores (Fig. 6).

Experimental glaucoma in rhesus monkeys allows for the study of pathophysiological changes in ocular structure and a comparison with a normal fellow eye as a control.[39–43] Our results concur with a prior *in vivo* study showing increase in area and elongation of laminar pores with advancing glaucoma.[32] That study compared human subjects divided into groups of normal, mild-moderate glaucoma, and severe-end-stage glaucoma. Here we compared eyes with experimental glaucoma with their own fellow eye as a normal control, hence eliminating inter-subject variability. Previous histological studies have clearly shown that with advancing glaucoma there is posterior bowing of the laminar surface.[4,5,13–17] We did not, in this study, measure position of the lamina cribrosa. We have observed, however, that greater defocus was required to visualize the laminar surface in glaucomatous eyes than in their normal fellow eyes, indicating that the laminar surface in glaucomatous eyes may be posterior compared with the laminar surface in normal fellow eyes. This difference in laminar position may contribute to a certain unknown extent to a decrease in average pore area, because if the actual size of the pores were unchanged after posterior bowing, then the measured pores would occupy a smaller area in pixels; i.e., the artifact caused by distance differences would be in the opposite direction. The observed increase in area may actually be an increase in physical size of pores or due to thinning of the laminar beam between the pores or fusion of adjacent pores.[13–17] Posterior bowing of the laminar surface may cause laminar pores, especially those at the periphery of the disc, to be imaged at an angle. Therefore it is possible that in some cases circular pores may be observed to be elongated. Longitudinal measures of lamina cribrosa will help to better understand such early structural changes. Longitudinal measurement of structural changes will provide important information about the nature of the stresses on the laminar surface. Such data would be beneficial to modeling studies of laminar structural changes that currently use *in vitro* measurements.[13,17,46] In any case, the morphological parameters presented here adequately reflect changes in laminar structure irrespective of whether they are direct or indirect.

The lamina cribrosa has been imaged in a primate eye with high resolution using the AOSLO, to our knowledge for the first time. Changes in area, elongation, and nearest-neighbor distance are manifestations of structural changes in the lamina associated with glaucoma. The preliminary data presented here provide the foundation for future studies of longitudinal changes in the laminar morphology associated with experimental glaucoma. For example, in studies of laminar morphological changes in experimental glaucoma, structural changes can be compared with functional measures such as electroretinography and perimetry to obtain a timeline of pathophysiological changes in glaucoma.[47] The AOSLO may be used not only in monitoring disease progression but also to assess the efficacy of therapeutic intervention in glaucoma.[48,49] Ultimately, AOSLO may be used to detect early structural changes in the lamina cribrosa in humans with glaucoma, possibly leading to earlier interventions and hence better prognosis.

ACKNOWLEDGMENTS

The corresponding author's e-mail address is vilupuru_abhiram@allergan.com.

*Current address, Allergan, Inc., RD3-2C, 2525 Dupont Drive, Irvine, California 92612.

†Current address, Room 485 Minor Hall, School of Optometry, University of California, Berkeley, Berkeley, California 94720-2020.

REFERENCES

1. J. M. Emery, D. Landis, D. Paton, M. Boniuk, and J. M. Craig, "The lamina cribrosa in normal and glaucomatous eyes," Trans.-Am. Acad. Ophthalmol. Otolaryngol. **78**, 290–297 (1974).
2. M. E. Yablonski and A. Asamoto, "Hypothesis concerning the pathophysiology of optic nerve damage in open angle glaucoma," J. Glaucoma **2**, 119–127 (1993).
3. J. B. Jonas, E. Berenshtein, and L. Holbach, "Anatomic relationship between lamina cribrosa, intraocular space, and cerebrospinal fluid space," Invest. Ophthalmol. Visual Sci. **44**, 5189–5195 (2003).
4. H. A. Quigley and W. Richard Green, "The histology of human glaucoma cupping and optic nerve damage: clinicopathologic correlation in 21 eyes," Ophthalmology **86**, 1803–1830 (1979).
5. H. A. Quigley, R. W. Flower, E. M. Addicks, and D. S.

McLeod, "The mechanism of optic nerve damage in experimental acute intraocular pressure elevation," Invest. Ophthalmol. Visual Sci. **19**, 505–517 (1980).

6. H. A. Quigley, E. M. Addicks, W. Richard Green, and A. E. Maumenee, "Optic nerve damage in human glaucoma II. The site of injury and susceptibility to damage," Arch. Ophthalmol. (Chicago) **99**, 635–649 (1981).

7. H. A. Quigley, R. M. Hohman, E. M. Addicks, R. W. Massof, and W. Richard Green, "Morphologic changes in the lamina cribrosa correlated with neural loss in open-angle glaucoma," Am. J. Ophthalmol. **95**, 673–691 (1983).

8. H. A. Quigley, A. Brown, and M. E. Dorman-Pease, "Alterations in elastin of the optic nerve head in human and experimental glaucoma," Br. J. Ophthamol. **75**, 552–557 (1991a).

9. H. A. Quigley, M. E. Dorman-Pease, and A. E. Brown, "Quantitative study of collagen and elastin of the optic nerve head and sclera in human and experimental monkey glaucoma," Curr. Eye Res. **10**, 877–888 (1991b).

10. M. R. Hernandez, W. M. Andrzejewska, and A. H. Neufeld, "Changes in the extracellular matrix of the human optic nerve head in primary open-angle glaucoma," Am. J. Ophthalmol. **109**, 180–188 (1990).

11. M. R. Hernandez, "The optic nerve head in glaucoma: role of astrocytes in tissue remodeling," Prog. Ret. Eye Res. **19**, 297–321 (2000).

12. J. D. O. Pena, P. A. Netland, I. Vidal, D. A. Dorr, A. Rasky, and M. R. Hernandez, "Elastosis of the lamina cribrosa in glaucomatous optic neuropathy," Exp. Eye Res. **67**, 517–524 (1998).

13. A. J. Bellezza, R. T. Hart, and C. F. Burgoyne, "The optic nerve head as a biomechanical structure: initial finite element modeling," Invest. Ophthalmol. Visual Sci. **41**, 2991–3000 (2000).

14. C. F. Burgoyne and J. C. Morrison, "The anatomy and pathophysiology of the optic nerve head in glaucoma," J. Glaucoma **10** (Suppl. 1), S16–S18 (2001).

15. A. J. Bellezza, C. J. Rintalan, H. W. Thompson, J. C. Downs, R. T. Hart, and C. F. Burgoyne, "Deformation of the lamina cribrosa and anterior scleral canal wall in early experimental glaucoma," Invest. Ophthalmol. Visual Sci. **44**, 623–637 (2003).

16. J. C. Downs, J.-K. F. Suh, K. A. Thomas, A. J. Bellezza, R. T. Hart, and C. F. Burgoyne, "Viscoelastic material properties of the peripapillary sclera in normal and early-glaucomatous monkey eyes," Invest. Ophthalmol. Visual Sci. **46**, 540–546 (2005).

17. C. F. Burgoyne, J. C. Downs, A. J. Bellezza, J.-K. F. Suh, and R. T. Hart, "The optic nerve head as a biomechanical structure: a new paradigm for understanding the role of IOP-related stress and strain in the pathophysiology of glaucomatous optic nerve head damage," Prog. Ret. Eye Res. **24**, 39–73 (2005).

18. D. R. Anderson and A. Hendrickson, "Effect of intraocular pressure on rapid axoplasmic transport in monkey optic nerve," Invest. Ophthalmol. **13**, 771–783 (1974).

19. H. A. Quigley and R. Anderson "The dynamics and location of axonal transport blockade by acute intraocular pressure elevation in primate optic nerve," Invest. Ophthalmol. **15**, 606–616 (1976).

20. D. S. Minckler, A. H. Bunt, and G. W. Johanson, "Orthograde and retrograde axoplasmic transport during acute ocular hypertension in the monkey," Invest. Ophthalmol. Visual Sci. **16**, 426–441 (1977).

21. R. L. Radius, "Distribution of pressure-induced fast axonal transport abnormalities in primate optic nerve: an autoradiographic study," Arch. Ophthalmol. (Chicago) **99**, 1253–1257 (1981a).

22. R. L. Radius, "Regional specificity in anatomy at the lamina cribrosa," Arch. Ophthalmol. (Chicago) **99**, 478–480 (1981b).

23. R. L. Radius and B. Bade, "Axonal transport interruption and anatomy at the lamina cribrosa," Arch. Ophthalmol. (Chicago) **100**, 1661–1664 (1982).

24. D. S. Minckler, "Correlations between anatomic features and axonal transport in primate optic nerve head," **84**, 429–452 (1986).

25. J. E. Morgan, G. Jeffery, and A. J. E. Foss, "Axon deviation in the human lamina cribrosa," Br. J. Ophthamol. **82**, 680–683 (1998).

26. G. Tezel, K. Trinkaus, and M. B. Wax, "Alterations in the morphology of lamina cribrosa pores in glaucomatous eyes," Br. J. Ophthamol. **88**, 251–256 (2004).

27. J. Morgan-Davies, N. Taylor, A. R. Hill, P. Aspinall, C. J. O'Brien, and A. Azuara-Blanco, "Three dimensional analysis of the lamina cribrosa in glaucoma," Br. J. Ophthamol. **88**, 1299–1304 (2004).

28. H. Maeda, M. Nakamura, and M. Yamamoto, "Morphometric features of laminar pores in lamina cribrosa observed by scanning laser ophthalmoscopy," Jpn. J. Ophthalmol. **43**, 415–421 (1999).

29. F. W. Fitzke, H. Woon, G. T. Timberlake, L. Robinson, J. Marshal, and A. C. Bird, "Optical modifications to a scanning laser ophthalmoscope for high magnification, narrow optical section imaging," Lasers Light Ophthalmology **4**, 7–14 (1991).

30. W. H. Woon, F. W. Fitzke, A. C. Bird, and J. Marshall, "Confocal imaging of the fundus using a scanning laser ophthalmoscope," Br. J. Ophthamol. **76**, 470–474 (1992).

31. A. Bhandari, L. Fontana, F. W. Fitzke, and R. A. Hitchings, "Quantitative analysis of the lamina cribrosa *in vivo* using a scanning laser opthlamoscope," Curr. Eye Res. **16**, 1–8 (1997).

32. L. Fontana, A. Bhandari, F. W. Fitzke, and R. A. Hitchings, "*In vivo* morphometry of the lamina cribrosa and its relation to visual field loss in glaucoma," Curr. Eye Res. **17**, 363–369 (1998).

33. J. Liang and D. R. Williams, "Aberrations and retinal image quality of the normal human eye," J. Opt. Soc. Am. A **14**, 2873–2883 (1997).

34. A. Roorda, F. Romero-Borja, W. J. Donnelly, H. Queener, T. Hebert, and M. Campbell, "Adaptive optics scanning laser ophthalmoscopy," Opt. Express **10**, 405–412 (2002).

35. K. Venkateswaran, A. Roorda, and F. Romero-Borja, "Theoretical modeling and evaluation of the axial resolution of the adaptive optics scanning laser ophthalmoscope," J. Biomed. Opt. **9**, 132–138 (2004).

36. F. Romero-Borja, K. Venkateswaran, A. Roorda, and T. Hebert, "Optical slicing of human retinal tissue *in vivo* with the adaptive optics scanning laser ophthalmoscope," Appl. Opt. **44**, 4032–4040 (2005).

37. S. Poonja, S. Patel, L. Henry, and A. Roorda, "Dynamic visual stimulus presentation in an adaptive optics scanning laser ophthalmoscope," J. Refract. Surg. **21**, S575–580 (2005).

38. J. Martin and A. Roorda, "Direct and noninvasive assessment of parafoveal capillary leukocyte velocity," Ophthalmology **112**, 2219–2224 (2005).

39. R. S. Harweth, E. L. Smith III, and L. DeSantis, "Experimental glaucoma: perimetric field defects and intraocular pressure," J. Glaucoma **6**, 390–401 (1997).

40. R. S. Harweth, L. Carter-Dawson, F. Shen, E. L. Smith III, and M. L. J. Crawford, "Ganglion cell losses underlying visual field defects from experimental glaucoma," Invest. Ophthalmol. Visual Sci. **40**, 2242–2250 (1999).

41. R. S. Harweth, M. L. J. Crawford, L. J. Frishman, S. Viswanathan, E. L. Smith III, and L. Carter-Dawson, "Visual field defects and neural losses from experimental glaucoma," Prog. Ret. Eye Res. **21**, 91–125 (2002).

42. D. Gaasterland and C. Kupfer, "Experimental glaucoma in the rhesus monkey," Invest. Ophthalmol. **13**, 455–457 (1974).

43. L. J. Frishman, F. Shen, L. Du, J. G. Robson, R. S. Harweth, E. L. Smith III, L. Carter-Dawson, and M. L. J. Crawford, "The scotopic electroretinogram of macaque after retinal ganglion cell loss from experimental glaucoma," Invest. Ophthalmol. Visual Sci. **37**, 125–141 (1996).

44. P. J. Diggle, *Statistical Analysis of Spatial Point Patterns* (Academic, 1983).

45. A. G. Bennett, A. R. Rudnicka, and D. F. Edgar, "Improvements on Littmann's method of determining the

size of retinal features by fundus photography," Graefe's Arch. Clin. Exp. Ophthalmol. **232**, 361–367 (1994).

46. I. A. Sigal, J. G. Flanagan, and C. Ross Ethier, "Factors influencing optic nerve head biomechanics," Invest. Ophthalmol. Visual Sci. **46**, 4189–4199 (2005).

47. S. Viswanathan, L. J. Frishman, J. G. Robson, R. S. Harwerth, and E. L. Smith III, "The photopic negative response in the macaque electroretinogram is reduced by experimental glaucoma," Invest. Ophthalmol. Visual Sci. **40**, 1124–1136 (1999).

48. E. WoldeMussie, G. Ruiz, M. Wijono, and L. A. Wheeler, "Neuroprotection of retinal ganglion cells by brimonidine in rats with laser-induced chronic ocular hypertension," Invest. Ophthalmol. Visual Sci. **42**, 2849–2855 (2001).

49. W. A. Hare, E. WoldeMussie, R. N. Weinreb, H. Ton, G. Ruiz, M. Wijono, B. Feldmann, L. Zangwill, and L. Wheeler, "Efficacy and safety of memantine treatment for reduction of changes associated with experimental glaucoma in monkey, II: structural measures," Invest. Ophthalmol. Visual Sci. **45**, 2640–2651 (2004).